Journal of Marine Science and Engineering

MDPI

Article

The Temperature-Dependent Monotonic Mechanical Characteristics of Marine Sand–Geomembrane Interfaces

Zhiming Chao [1,2,3,†], Hongyi Zhao [1,4,†], Hui Liu [3,†], Peng Cui [2], Danda Shi [3], Hai Lin [5], Yang Lu [1], Bing Han [6] and Shuang Chen [7,*]

1 Hohai University, Nanjing 210098, China; zmchao@shmtu.edu.cn (Z.C.); aftao@hhu.edu.cn (H.Z.); luy@hhu.edu.cn (Y.L.)
2 College of Civil Engineering, Nanjing Forestry University, Nanjing 210037, China; cui@njfu.edu.cn (P.C.)
3 College of Ocean Science and Engineering, Shanghai Maritime University, Shanghai 200135, China; ll1668827009@163.com (H.L.); ddshi@shmtu.edu.cn (D.S.)
4 Qingdao University of Technology, Qingdao 266525, China
5 College of Architecture and Engineering, Nanchang University, Nanchang 330031, China; linhai@ncu.edu.cn
6 Shanghai Ship and Shipping Research Institute Co., Ltd., Shanghai 200135, China; han.bing@coscoshipping.com
7 Jiangsu Province Water Engineering Sci-tech Consulting Co., Ltd., Nanjing 210029, China
* Correspondence: 18805162620@139.com
† These authors contributed equally to this work.

Abstract: The utilization of geomembrane reinforcement technology is pervasive in marine sand foundation reinforcement projects. However, the elevated temperatures and intricate stress conditions prevalent in marine environments exert a notable influence on the mechanical characteristics of geomembrane interfaces comprising marine sand, which impedes the efficacy of geomembrane reinforcement in marine sand foundations. Nevertheless, there is a lack of research investigating the temperature-dependent interfacial mechanical performance of geomembranes and marine sand under diverse stress states. In this study, a series of monotonic shear tests were carried out on the interface between geomembranes and marine sand within a temperature range of 5 °C to 80 °C. These experiments were carried out using a self-developed large-scale temperature-controlled interfacial dynamic and static shear device. The experimental results demonstrate that temperature has a pronounced effect on the monotonic mechanical characteristics of the geomembrane–marine sand interface, which displays clear temperature dependence. The findings of this study may help in the design and optimization of offshore projects where a marine sand–polymer layer interface exists.

Keywords: temperature; marine sand; polymer layer; shear tests; peak shear strength

Citation: Chao, Z.; Zhao, H.; Liu, H.; Cui, P.; Shi, D.; Lin, H.; Lu, Y.; Han, B.; Chen, S. The Temperature-Dependent Monotonic Mechanical Characteristics of Marine Sand–Geomembrane Interfaces. *J. Mar. Sci. Eng.* **2024**, *12*, 2193. https://doi.org/10.3390/jmse12122193

Received: 3 November 2024
Revised: 25 November 2024
Accepted: 29 November 2024
Published: 30 November 2024

1. Introduction

Marine sand, a type common in subtropical and tropical coastal areas, has recently been employed with increasing frequency as a construction material for engineering facilities. These include foundations for islands and coral reefs in the South China Sea and tropical coastal facilities [1–4]. However, the presence of weak cementation, porosity, fragile particles, and other characteristics inherent to marine sand may result in uneven foundation settlement or local collapse when facilities are subjected to hydraulic infiltration and wave action in engineering applications, thereby posing a significant risk to the safety of marine engineering facilities [5,6]. Geomembrane reinforcement technology is a widely employed method in marine sand engineering, serving as an effective reinforcement technique to prevent the uneven settlement of foundations [7–11]. The efficacy of geomembrane reinforcement is contingent upon the mechanical characteristics of the coral sand–

geomembrane interface. It is therefore essential to conduct a detailed study of the mechanical characteristics of the coral sand–geomembrane interface [12–18].

In engineering practice, subtropical and tropical coastal areas, characterized by high temperatures and the use of exothermic equipment, give rise to a temperature-changing environment. This, in turn, affects the marine sand–geomembrane interface [19–21]. To illustrate, the oil and gas that emanate from submarine pipelines can reach temperatures of up to 80 °C, with the heat being continuously transferred to the surrounding coral sand. Additionally, due to the intense solar radiation and elevated temperatures characteristic of tropical coastal areas, the surface temperature of coral sand engineering equipment may reach 70 °C to 80 °C.

The raw materials employed in the manufacture of geomembranes are predominantly synthetic polymers, including polystyrene, polyethylene, and polypropylene. These are thermoplastic materials, the properties of which undergo alteration in response to temperature. The temperature modulus of HDPE can be expressed by the following Equation (1) [22–24].

$$E(T) = 1.300 \times 10^{-0.018T} \quad (1)$$

where T is the temperature in degrees Celsius, and the temperature modulus, E, is in MPa. It can be seen that the temperature modulus of HDPE continuously decreases with increasing temperature. At elevated temperatures, geomembranes undergo a softening process, which subsequently results in a weakening of their mechanical characteristics [25–29]. The extant literature indicates that an increase in temperature will result in a change in the shear failure mode of the geomembrane. This will decrease the tensile strength of the non-woven fibers, and the damage to the geomembrane's needled fibers will undergo a shift from pull-out damage to tensile damage [30]. For instance, it has been demonstrated that geomembranes' tensile strength and modulus of elasticity undergo a decrease of approximately 30% when temperature rises from 20 °C to 60 °C [31–33]. With regard to the mechanical performance of coral sands in response to temperature, it has been demonstrated that temperature influences the mobility of pore water in the soil, which in turn alters the pore water pressure and thus induces a change in the effective soil stress [34–37]. Furthermore, temperature has been demonstrated to influence the cementation between soil particles, thereby modifying the soil structure [38–44]. These two factors result in a considerable impact of temperature on the mechanical characteristics of coral sand. The alterations in the mechanical characteristics of the geomembrane and coral sand result in a coupling effect that has a considerable impact on the mechanical characteristics of the coral sand–geomembrane interface. Nevertheless, the absence of temperature-controlled interfacial shear instrumentation has resulted in a shortage of studies examining temperature-dependent alterations in the mechanical performance of coral sand–geosynthetic interfaces. A limited number of studies have investigated the mechanical response of the indigenous sand (silica sand)–geomembrane interface over temperature ranges of 3 °C to 42 °C and 21 °C to 50 °C [45]. However, in contrast to terrestrial sand, marine sand is characterized by irregular particle shape, a porous structure, and friable particles, which give rise to notable differences between the mechanical response of the terrestrial sand–geomembrane interface and that of the coral sand–geomembrane interface [46–50]. It is therefore essential to investigate the mechanical characteristics of the marine sand–geomembrane interface in the context of temperature changes. The stability of marine facilities is dependent on a stable foundation; due to its joint action with shear load temperature, the shear dilation angle of the sand–geosynthetic interface will change in actual use, which in turn affects the risks associated with the foundation's stress distribution, and the stability of marine facilities. Therefore, it is necessary to study the shear dilation angle of the sand–geotechnical mold interface at different temperatures.

Marine engineering installations are typically exposed to a wide range of stress loads, including monotonic shear and normal-phase loads induced by waves, earthquakes, and

vehicles [51,52]. Moreover, the viscoelastic nature of the soil–geomembrane interface results in notable alterations in the mechanical performance of the interface between marine sands and geomembranes in response to changes in stress [53,54]. It was established that the interfacial mechanical response to monotonic shear experiments at varying loads exhibited distinct characteristics for soil and geosynthetics. Additionally, the damage threshold of the interface exhibited discrepancies under varying normal loads, with the interface subjected to greater normal loads demonstrating a heightened susceptibility to damage [55–57]. Furthermore, existing studies have shown notable discrepancies in the mechanical characteristics of soil–geosynthetic interfaces subjected to disparate monotonic shear loading conditions [58–61]. Nevertheless, there is a lack of research examining the temperature-dependent mechanical response of marine sand and geosynthetic interfaces under varying loads. Additionally, there is a lack of studies that have considered the mechanical characteristics of monotonic interfaces in the context of temperature effects.

This paper carried out a series of monotonic shear tests on marine sand and geomembranes using a self-developed temperature-controlled apparatus capable of dynamic and static shear testing. To simulate the actual state of the upper layer of sandy soil on a foundation, which is sensitive to temperature, everyday stress levels of 20 kPa, 35 kPa, and 50 kPa were chosen. The tests were conducted over a temperature range of 5 °C to 80 °C. The test results permit an analysis and comparison of the mechanical properties of marine sand–geomembrane interfaces subjected to monotonic shear loading. The findings of this study can inform the design of coral sand–geomembrane interfaces in marine engineering facilities and serve as a point of reference for the construction of future marine projects.

2. Experiments

2.1. Experimental Apparatus

In this study, temperature-controlled monotonic shear tests were conducted on marine sand–geomembrane interfaces using a self-developed apparatus for interfacial dynamic and static shear testing. The apparatus was designed to accommodate large samples and to maintain precise temperature control. The apparatus consists of an external ambient temperature cabinet with an interfacial shear system mounted inside. The system is designed for use in a wide range of applications. The temperature can be maintained at a constant level within a range of −50 °C to 200 °C over an extended period (7 days) during the course of experiments [62].

2.2. Materials

2.2.1. Marine Sand

This paper used marine sand with a particle size of 1 mm~2 mm as the experimental material. Scanning electron microscope (SEM) observation was carried out on the marine sand, and the scanning results are shown in Figure 1. The maximum dry density of the marine sand used in the experiments as obtained from Proctor tests was 1.75 g/cm^3, and the optimum water content was 9.65%. The pertinent parameters of the sand samples employed in the experiment are illustrated in Figure 1 and Table 1. SP sand is defined in ASTM D2487 [63] as pure sand with a coefficient of uniformity (Cu) of less than 6 or a coefficient of curvature (Cc) of less than 1. The rationale behind the use of SP sand in the experiments was to mitigate the impact of grading effects. The marine sand used in this experiment is poorly graded sea sand, SP sand, according to ASTM D2487.

Table 1. The parameters of the soil.

Soil	Parameters	Value
coral sand	Particle size range (mm)	1~2
	Maximum dry density (g/cm^3)	1.75
	D_{10}	1.03

D_{30}	1.09
D_{50}	1.17
Optimum water content (%)	9.65
Coefficient of uniformity (C_u)	1.46
Coefficient of curvature (C_c)	0.94

The extant literature indicates that sand grain size exerts a discernible influence on the mechanical characteristics of a sand–structure interface [64,65]. Most existing studies on marine sand grain size concentrate on a range from 1 mm to 2 mm [66–69]. Accordingly, the particle sizes of marine sand selected in this paper are between 1 mm and 2 mm to reduce the particle size effect [70–72].

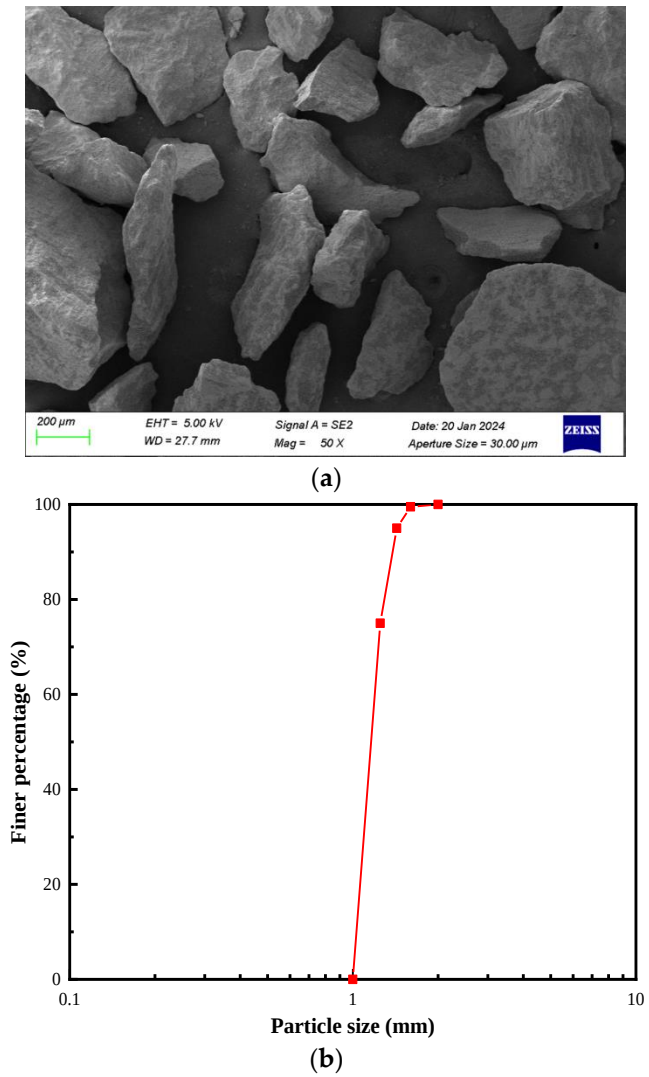

Figure 1. Marine sand SEM images. (**a**) The SEM images. (**b**) Particle size distribution.

2.2.2. Geomembrane

In this study, a rough geomembrane manufactured from high-density polyethylene (HDPE) was used, as shown in Figure 2. The specific parameters of the geomembrane are shown in Table 2. The tensile strength and resilience of the HDPE geomembrane is superior to that of other polymers. Moreover, the HDPE geomembrane exhibits excellent corrosion resistance and anti-aging properties, which have led to its widespread utilization in a variety of marine facilities [73–75].

Table 2. The parameters of the geomembrane.

Parameters	Value
Thickness (mm)	1.5
Density (g/cm^3)	0.942
Fracture strength (N/mm)	16.3
Yield strength (N/mm)	22.4
Yield elongation rate (%)	12.3
Fracture elongation rate (%)	120
Melting temperature (°C)	134
Melt flow index (g/min)	0.4
Melt flow ratio (—)	123 ± 3
Puncture strength (N)	402

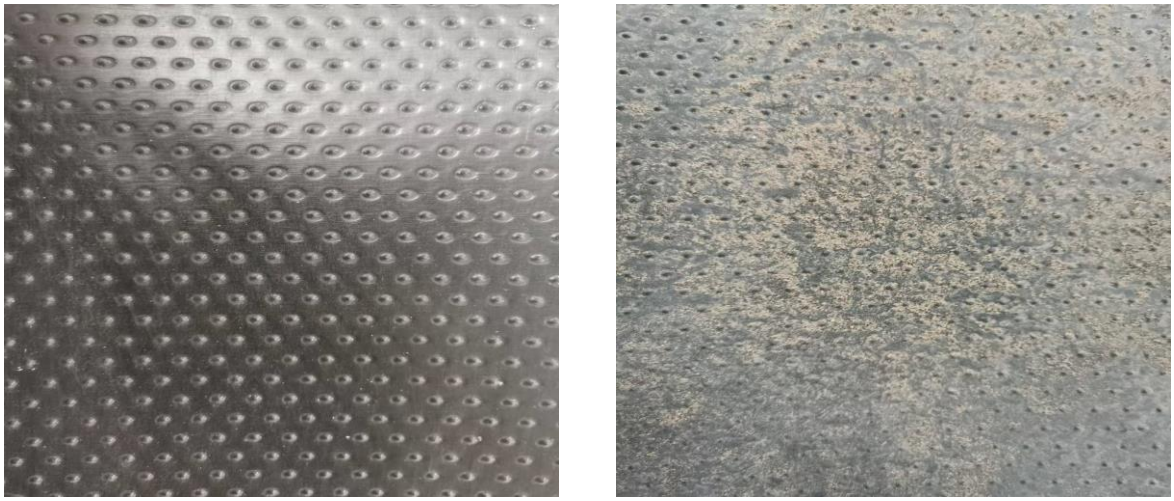

(**a**) (**b**)

Figure 2. HDPE geomembrane. (**a**) pre-experimental (**b**) post-experimental

2.3. Experimental Procedure

In this research study, we used a large temperature-controlled shear apparatus to conduct a direct shear experiment on the marine sand–geomembrane interfaces, and the adopted test procedure is based on the requirements of ASTM D5321M-21 [76]. Additionally, in existing research on interface shear tests, similar experimental methods to those used in our research were applied, which indicates the applicability of our adopted experimental procedure [77–81]. It also demonstrates the reliability of our experimental results.

The dimensions of the geomembrane sample were 460 mm in length and 280 mm in width. These dimensions were derived in accordance with the specifications outlined in ASTM D 6072[82]. In the experiment, the geomembrane specimen was fixed, textured-side up, to the front of the lower shear box. Shearing was then applied along the length of the sample. The marine sand sample was placed into the upper shear box at a thickness of 100 mm, with the optimum moisture content. Shearing between the marine sand and the geomembrane was achieved by fixing the upper shear box and moving the lower shear box.

Upon the installation of the coral sand and geomembrane samples, the external ambient temperature cabinets were sealed, and the internal temperature of the cabinets was adjusted to a specified value. In this study, temperatures of 5 °C, 20 °C, 40 °C, 60 °C, and 80 °C were employed. Subsequently, everyday stress was applied to the marine sand–geomembrane interfaces by the upper loading plate on the soil sample, with normal stress levels of 20 kPa, 35 kPa, and 50 kPa being utilized. Following the consolidation of the soil sample under normal stress for three hours, shearing was initiated on the marine sand–

geomembrane interfaces. Monotonic displacement-controlled rapid shear experiments were conducted at 1 mm per minute. In the case of monotonic shear, the interface underwent a unidirectional shear displacement of 100 mm. The shear stress changes and displacements at the marine sand–geomembrane interface were observed and recorded by normal and horizontal sensors throughout the shear experiments. The specific experimental scheme is outlined in Table 3.

Table 3. Experimental scheme.

Experiment Type	Cement Mortar Thickness (mm)	Normal Stress (kPa)	Shear Rate (mm/min)	Shear Amplitude (mm)	Temperature (°C)
Monotonic direct shear test	10.0	20 35 50	1.0	50.0	5 20 40 60 80

3. Results and Analysis

3.1. The Temperature-Dependent Interfacial Mechanical Response Under Monotonic Shear Loading

The curves of shear stress and vertical displacement versus shear displacement under monotonic shear loading at different temperatures are shown in Figure 3, while the relationship curve of peak interfacial shear strength with temperature under monotonic shear loading is shown in Figure 4.

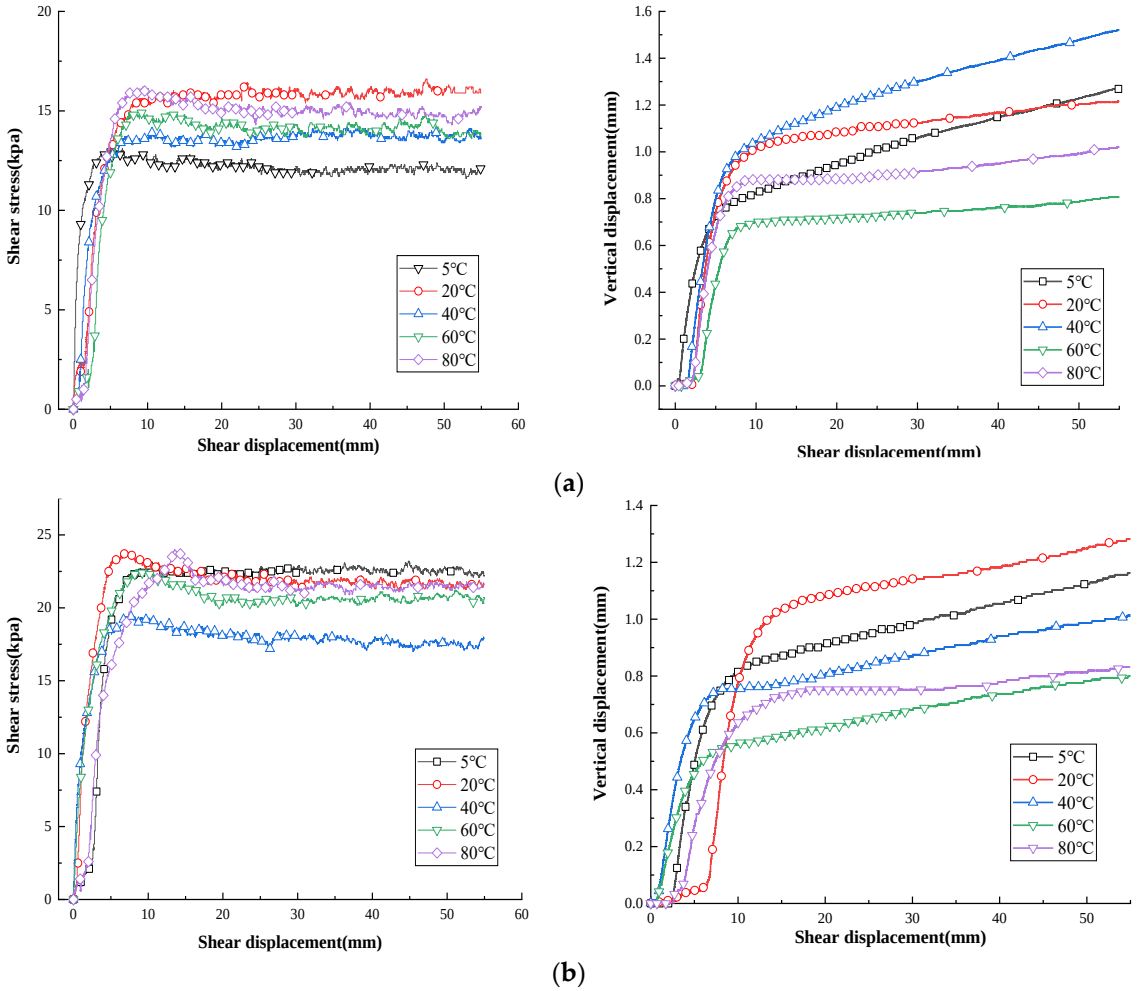

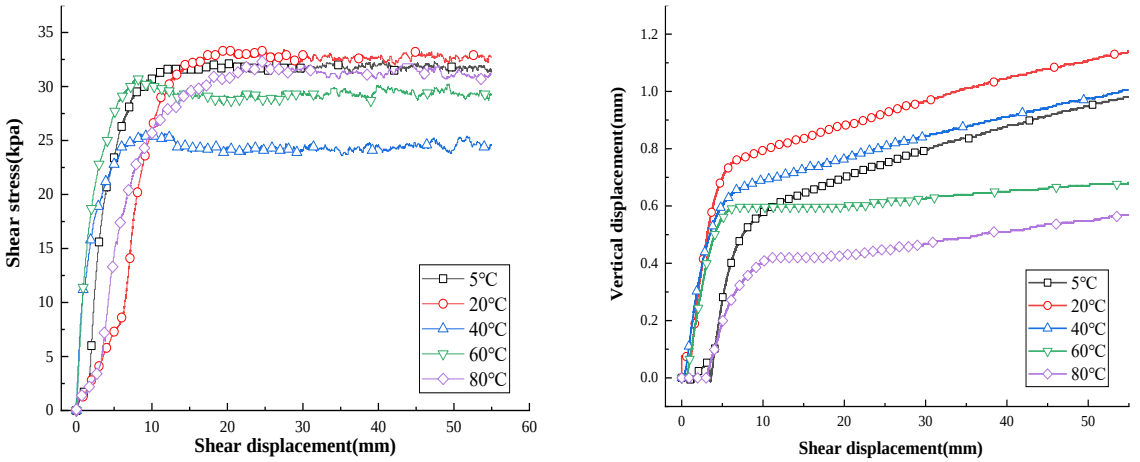

(**c**)

Figure 3. Curves of shear stress and vertical displacement versus shear displacement under monotonic shear loading. (**a**) Normal stress—25 kPa; (**b**) normal stress—35 kPa; (**c**) normal—stress 50 kPa.

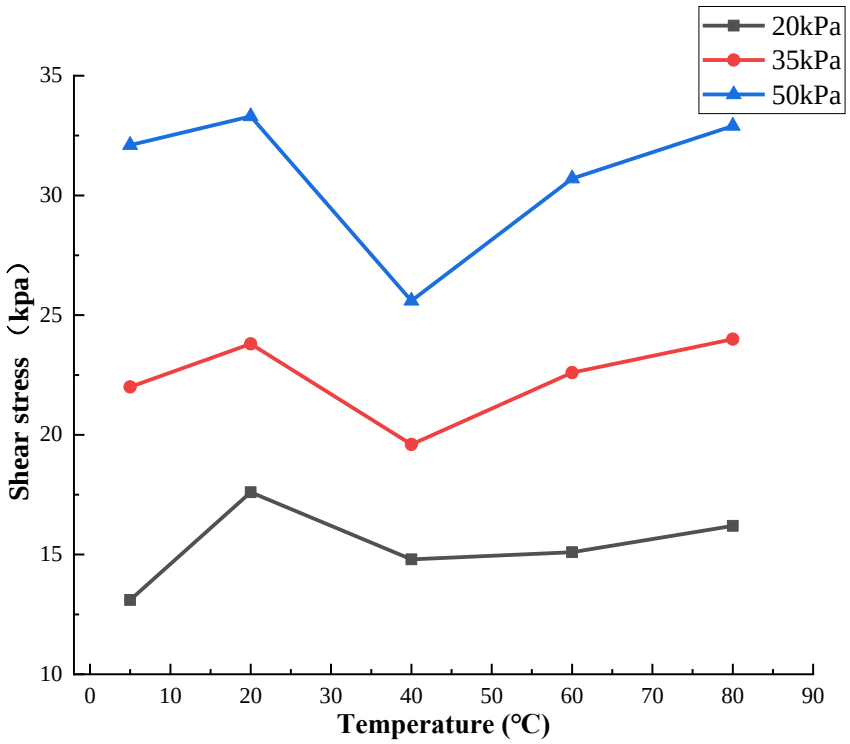

Figure 4. Relationship curves of peak interfacial shear strength with temperature.

Figures 3 and 4 show that the shear stress versus displacement curves at the marine sand–geomembrane interface exhibit temperature-dependent behavior at different normal stress. Additionally, the variation rules governing the mechanical response of the interface are analogous and dependent on the temperature extent, with the specific values dependent on the normal stress levels applied. In particular, an increase in peak shear strength is observed within the temperature ranges of 5 °C to 20 °C and 40 °C to 80 °C, while a decrease in peak shear strength is observed within the temperature range of 20 °C to 40 °C. To illustrate, under 20 kPa of normal stress, the peak interfacial shear strength demonstrates an increase from 13.2 kPa to 17.6 kPa and from 14.8 kPa to 16.2 kPa across the temperature ranges of 5 °C to 20 °C and 40 °C to 80 °C, respectively. Inversely, within the temperature range of 20 °C to 40 °C, there is a decline in the interface's peak shear strength from 17.6 kPa to 14.8 kPa.

Moreover, the interface's peak shear strength demonstrates heightened susceptibility to temperature fluctuations within the 20 °C to 40 °C range compared to other temperature ranges. To illustrate, under 50 kPa of normal stress, the interface's peak shear strength exhibits a 23.12% reduction from 33.3 kPa to 25.6 kPa as the temperature increases from 20 °C to 40 °C. Inversely, the interface's peak shear strength demonstrates a 3.74% increase from 32.1 kPa to 33.3 kPa and a 19.92% increase from 25.6 kPa to 30.7 kPa as the temperature rises from 5 °C to 20 °C and from 40 °C to 60 °C, respectively. In addition, the sensitivity of the peak interfacial shear strength to temperature change is shown to be higher under high positive stress conditions than under low positive stress conditions. This study considers the pattern of change in the peak shear strength of the interface in the temperature range of 40 °C to 60 °C. It is observed that there is a increase in the peak shear strength, at normal stress of 50 kPa, 35 kPa and 20 kPa, respectively, the peak interfacial shear strength varied as follows: from 25.6 kPa to 30.7 kPa, an increase of 19.92% from 19.6 kPa to 22.6 kPa an increase of 15.3% and from 14.8 kPa to 15.1 kPa an increase of 2.02%. The peak interfacial shear strength is generally observed to reach a maximum at 20 °C and a minimum at 40 °C at different normal stress levels. Additionally, the sensitivity of the peak shear strength to temperature fluctuations initially declines with rising temperatures, subsequently attains a nadir at 40 °C, and then resumes an upward trajectory.

This phenomenon could be attributed to the interlocking and sliding effects between marine sands and rough geomembranes, which are the primary factors contributing to the monotonic peak shear strength at the interface. The impact of temperature elevation on interlocking and sliding effects was observed to vary. Due to the geomembrane softening with an increase in temperature, the marine sand particles could be inserted deeper into it, which enhanced the interlocking effect and increased the monotonic peak shear strength of the interface. Inversely, as the surface protrusions of the geomembrane softened at elevated temperatures, the sliding effect between the marine coral sand and the textured geomembrane was diminished, resulting in a reduction in the peak shear strength of the interface. As the temperature rose from 5 °C to 20 °C, the geomembrane experienced softening due to normal-phase pressure and temperature. This led to the marine sand being embedded in the geomembrane, thereby enhancing the interlocking effect and increasing shear strength. As the temperature increased from 20 °C to 40 °C, the geomembrane experienced a further softening effect. The bumps on the surface of the geomembrane underwent significant wear, weakening the sliding effect at the interface between the marine sand and the geomembrane. At this point, the sliding effect was stronger than the interlocking effect, and the shear strength demonstrated a declining trend. As the temperature rose from 40 °C to 80 °C, the interlocking effect at the marine sand–geomembrane interface exhibited a continuous increase in strength, reaching a point where the enhancement of the interlocking effect surpassed the weakening of the sliding effect. This resulted in the observed tendency of the shear strength to increase.

An analysis of variance (ANOVA) was performed on the data presented in Figure 5 to verify whether temperature had a significant effect on the shear strength of the sand–geomembrane interface. The ANOVA equation used is as follows:

$$S^2 = \frac{1}{n-1}\sum_{i=1}^{n}(X_i - \bar{X})^2 \quad (2)$$

where $\bar{X}$ is the sample average, and n is the sample size.

As evidenced in Table 4, temperature exerts a pronounced influence on shear strength at varying normal pressure levels. Furthermore, the impact of temperature on shear strength intensifies in tandem with the rise in normal pressure.

Table 4. Sample variance .

Normal stress	25 kPa	35 kPa	50 kPa
Sample variance	2.242	2.512	7.866

The angle of internal friction and the cohesion of marine sand obtained by fitting the experimental shear strength data to the Coulomb strength theory are shown in Figures 5 and 6.

$$\tau = \mathrm{c} - \sigma \tan \varphi \tag{3}$$

where c represents the cohesion of marine sand, and φ represents the angle of friction of marine sand.

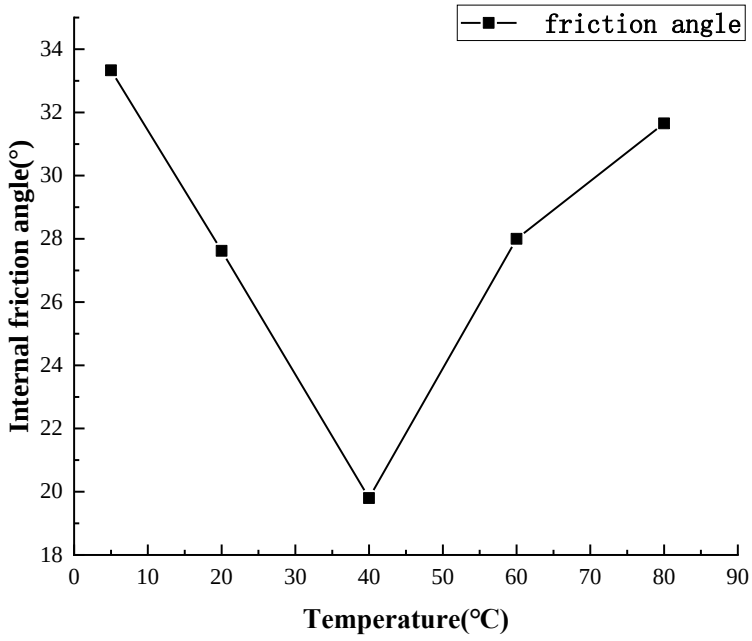

Figure 5. The peak internal friction angle versus temperature curve.

As illustrated in Figure 5, the variation in the friction angle at the marine sand–polymer layer interface is dependent on temperature. The friction angle demonstrates a continuous decrease from 5 °C to 40 °C, reaching a minimum value of 19.8°. As the temperature rises from 40 °C to 80°C, the friction angle increases from 19.8° to 31.7°, representing a 60% increase. Moreover, the sensitivity of the marine sand–polymer layer interface friction angle to temperature changes is observed to diminish as the temperature increases within a range of 40 °C to 80 °C.

As illustrated in Figure 6, the interfacial cohesion of marine sand–polymer layer interfaces exhibits temperature-dependent behavior. When the temperature rises from 5 °C to 40 °C, the cohesive force demonstrates a continuous increase from 1.33 kPa to 8.26 kPa. Conversely, as the temperature rises from 40 °C to 80 °C, the cohesion is observed to decrease to 4.55 kPa. The marine sand exhibits a diminished cohesive force in response to extreme temperature fluctuations.

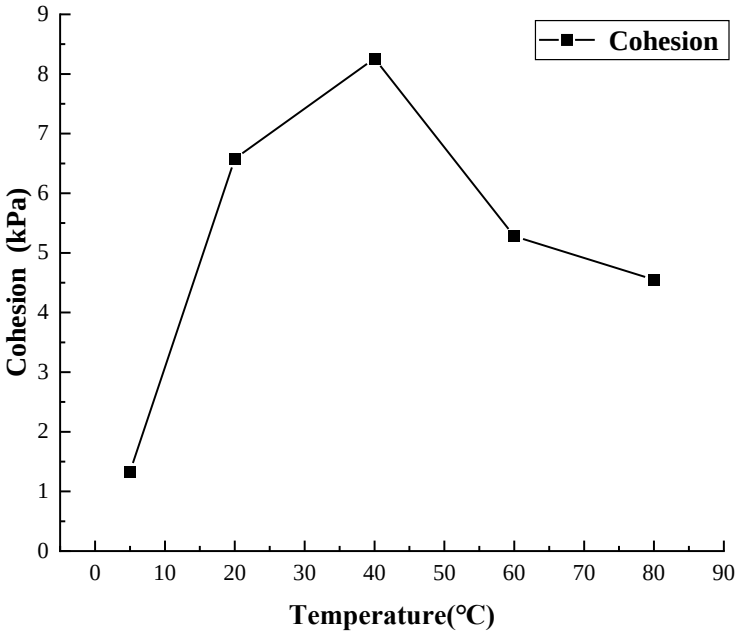

Figure 6. The relationship curve between cohesion and temperature.

3.2. The Temperature-Dependent Interface Dilation Angle Under Monotonic Shear Loading

The shear dilation angle reflects the change in the volume of the sandy soil in shear due to shear dilation, which is closely related to the change in normal displacement in shear. By adopting Equation (4) [83], we obtained relationship curves between temperature and shear dilation angle for the different normal pressure levels.

$$\xi = \tan^{-1}\left(\frac{\Delta v}{\Delta u}\right) \quad (4)$$

where Δv represents the incremental vertical displacement of the interface, and Δu represents the incremental horizontal displacement of the interface.

Figure 7 demonstrates that the alteration rules governing the interface dilation angle in response to temperature elevation for marine sand–polymer layer interfaces exhibit a comparable pattern and are contingent upon the extent of normal stress. Additionally, the change in the dilation angle at elevated temperatures at different normal stress levels is analogous to that of the interface's peak shear strength. In particular, the trend curve for the shear expansion angle with increasing shear displacement can be divided into two distinct segments. The first segment, which spans a shear displacement range of 0 mm to 10 mm, exhibits a positive correlation between shear displacement and shear dilation angle, reaching a peak value at a displacement of 10 mm. The second segment is defined by shear displacement values between 10 mm and 60 mm. During this period, the shear dilation angle decreases with increasing shear displacement.

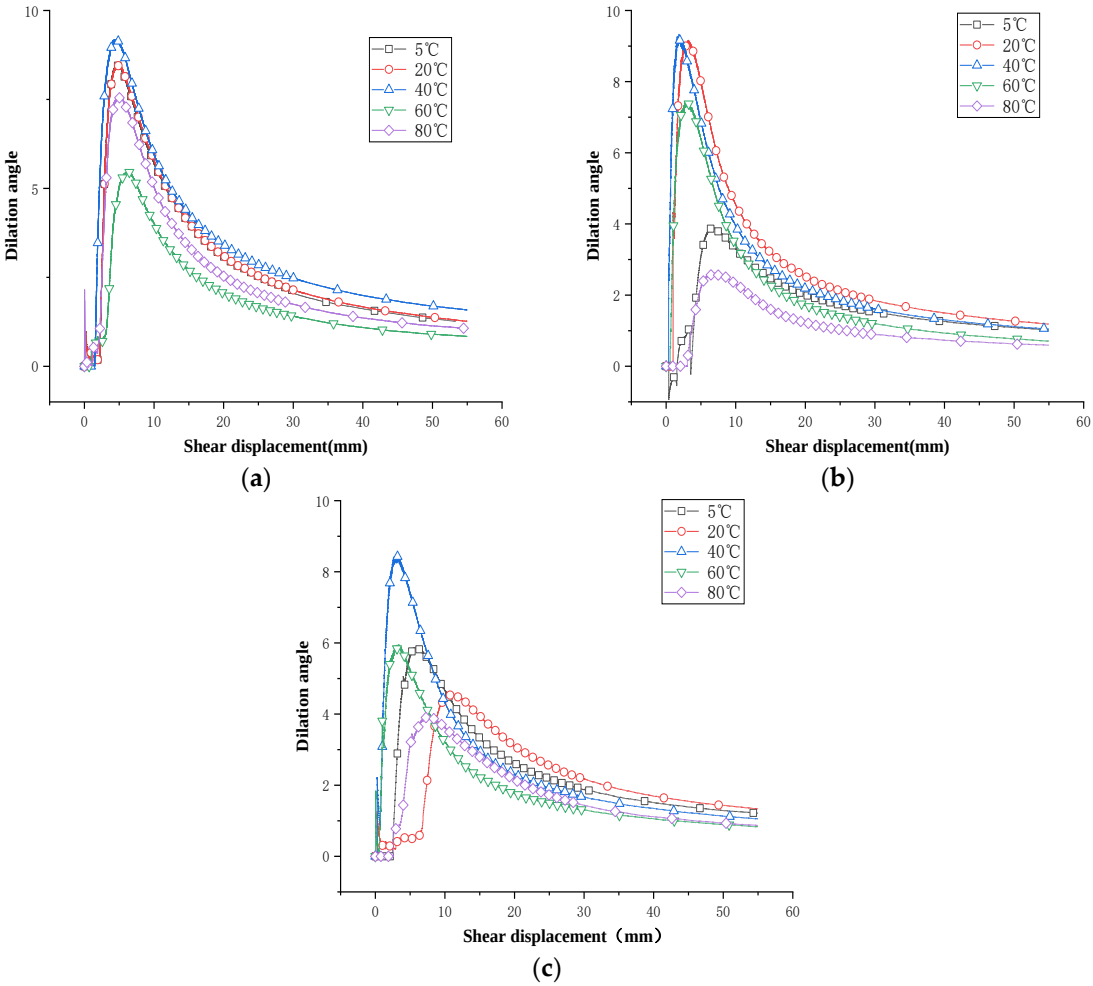

Figure 7. Relationship curves between the interface dilation angle and shear displacement. (**a**) Normal stress—20 kPa; (**b**) normal stress—35 kPa; (**c**) normal stress—50 kPa.

Figure 8 illustrates that the variation patterns of the maximum interface dilation angle with temperature fluctuations at the marine sand–polymer layer interface under different normal stress conditions are comparable, jointly determined by temperature and normal stress. In particular, the maximum shear expansion angle of the marine sand–polymer layer interface demonstrates temperature dependence, with an increase in temperature resulting in a corresponding increase in the angle. To illustrate, at 50 kPa, the maximum shear dilation angle decreased from 5.89° to 4° as the temperature increased from 5 °C to 20 °C. A reduction of 23% was noted in the maximum shear dilation angle, from 55° to 4.55°, with an increase in temperature from 20 °C to 40 °C. Subsequently, an 86% increase was observed in the aforementioned angle, reaching a peak of 8.46°. Upon further elevation of the temperature from 40 °C to 80 °C, a continuous decrease in the maximum shear dilation angle was observed, from 8.46° to 3.91°, representing a 54% reduction.

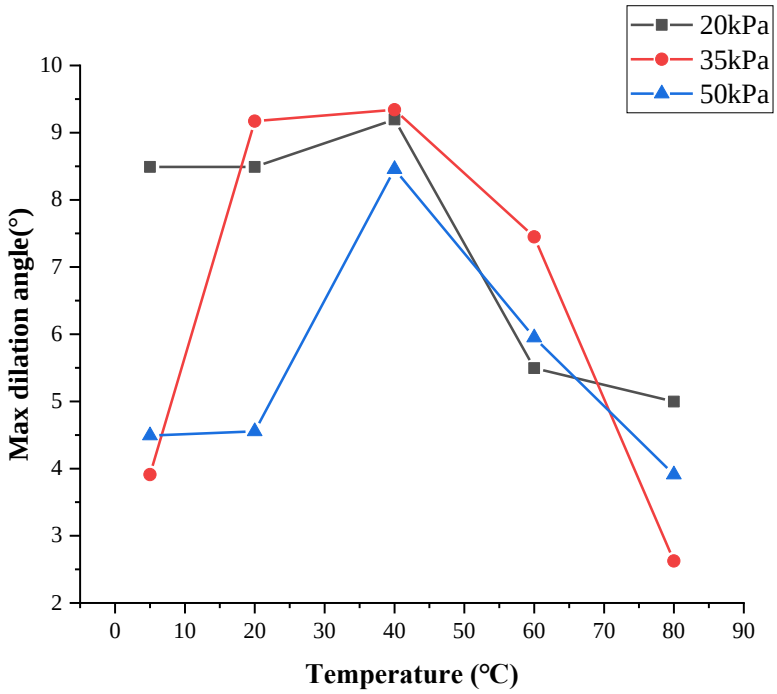

Figure 8. Relationship curves between the maximum interface dilation angle and temperature.

4. Discussion

This paper presents findings that indicate that an increase in the monotonic peak shear strength of the marine sand–textured geomembrane interface occurs within the temperature ranges of 5 °C to 20 °C and 40 °C to 80 °C. Conversely, the interface's peak shear strength is observed to decrease within the temperature range of 20 °C to 40 °C. This can be attributed to the interlocking and sliding effects between marine sand and the textured geomembrane, which are the primary factors responsible for generating the interface's monotonic peak shear strength [35]. The influence of temperature on interlocking and sliding effects varies. As a consequence of the geomembrane's softening at elevated temperatures, marine sand particles can be inserted more deeply into the geomembrane under the influence of normal stress, thereby enhancing interlocking effects and contributing to an increase in the interface's monotonic peak shear strength [84]. In contrast, the sliding effects between marine sand and the textured geomembrane are diminished due to the softening of protruding points on the geomembrane surface at elevated temperatures, which exerts a reducing influence on the interface's peak shear strength [85]. Moreover, the primary factors affecting the peak interfacial shear strength demonstrate notable variation across different temperature ranges [86,87]. In instances where the sliding effect is the principal factor influencing peak shear strength, an increase in temperature results in an enhancement of the peak interfacial shear strength. Inversely, when the interlocking effect is the primary determinant of peak shear strength, an increase in temperature results in a reduction in the peak shear strength of the interface [88,89]. As illustrated in Figure 9, the images of the geomembrane surface after monotonic shearing at various temperatures (5 °C, 20 °C, 40 °C, 60 °C, and 80 °C) reveal that the protruding points remain intact at temperatures of 5 °C and 20 °C. However, at temperatures of 40 °C, 60 °C, and 80 °C, the protruding point appears to be abraded, with a maximum vertical height of 0.03 mm, 0.08 mm, and 0.11 mm, respectively, and the depth of the scratches on the surface of the geomembrane becomes progressively deeper as the temperature increases, reaching a maximum depth of 0.23 mm at 80 °C. It can be reasonably deduced that the wear of the protruding points can significantly reduce sliding effects, given that sliding effects between

marine sand and textured geomembrane are mainly produced by the interaction between marine sand and the protruding points, as the wear of the protruding points occurs mainly in the temperature range of 20 °C to 40 °C. Therefore, an increase in temperature within the range of 20 °C to 40 °C results in a reduction in the monotonic peak interfacial shear strength due to the weakening of sliding effects. In contrast, within the temperature ranges of 5 °C to 20 °C and 40 °C to 80 °C, the marginal change in the dimensions and morphology of the protruding points results in interlocking effects becoming the primary factor influencing interaction at the interface. Accordingly, when temperatures rise within the specified temperature range, the intensification of interlocking effects leads to an augmentation in the interface's monotonic peak shear strength.

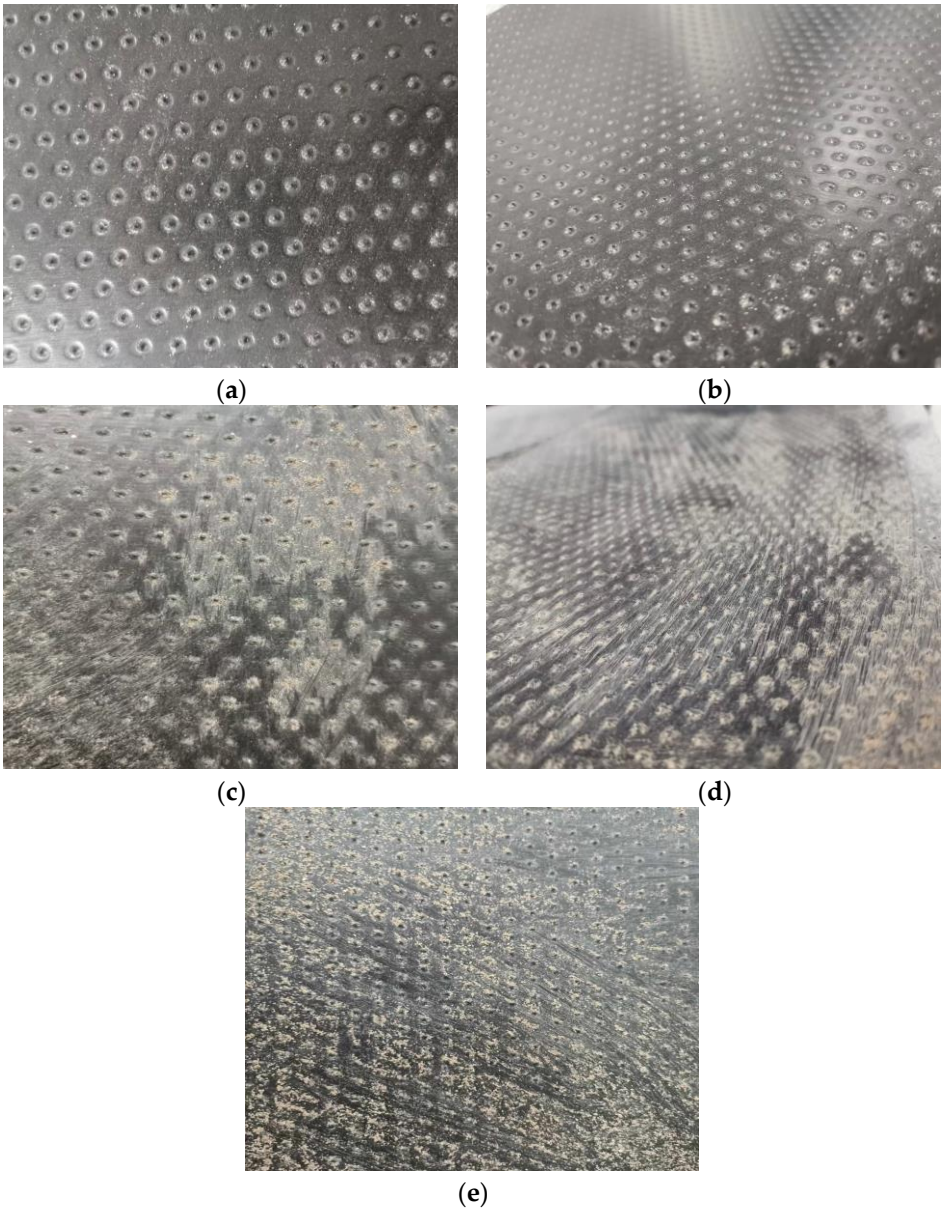

Figure 9. Photos of the textured surface geomembrane after testing at a normal pressure of 20 kPa. (**a**) Temperature—5 °C; (**b**) temperature—20 °C; (**c**) temperature—40 °C; (**d**) temperature—60 °C; (**e**) temperature—80°C.

Marine sand is a common sand type frequently employed in marine engineering applications. Therefore, the aim of this study was to investigate the effect of temperature on the mechanical properties of the interface between the polymer layer and the sand layer in offshore engineering, the temperature sensitivity of the shallow foundation structure

in offshore engineering, and the changes in the mechanical properties of the polymer layer and the sand layer when they are affected by high temperatures, so as to provide support for construction in offshore engineering in the future. To this end, marine sand was selected as the experimental material. It should be noted, however, that the shape of the sand grains and the geological conditions of marine sand affect the mechanical properties of marine sand. It should also be noted that the scope of this paper does not extend to an investigation of the effect of sand type and its geological conditions on the mechanical properties of the interface. Subsequently, further research will be conducted to investigate the influence of sand particle type and geological conditions on the mechanical properties of marine sand.

5. Conclusions

This paper presents the results of a series of temperature-controlled monotonic shear experiments on the marine sand–textured geomembrane interface, conducted at temperatures ranging from 5 °C to 80 °C. The experiments were conducted using a self-developed, large-scale, temperature-controlled interfacial monotonic shear device. The results of the temperature-controlled shear experiments were analyzed to determine the monotonic shear mechanical characteristics of marine sand–geomembrane interfaces at different stress levels. A series of analyses were conducted to evaluate the shear strength of the marine sand–geomembrane interface under a range of stress conditions. Additionally, introducing the shear expansion angle facilitated an investigation into the relationship between vertical and horizontal shear displacement. However, this paper does not expand the study of the shape of sand particles and geological conditions and their effects on the mechanical properties of the interface. This study therefore has certain limitations; in the future, we will carry out research on the shape of the sand and other aspects of the study to further explore the impact of temperature on the mechanical properties of the sand–geosynthetic interface.

The findings of our research demonstrate that the interfacial monotonic peak shear strength increases within the temperature ranges of 5 °C to 20 °C and 40 °C to 80 °C. Conversely, a decline in the interfacial peak shear strength is observed within the 20 °C to 40 °C temperature range. Furthermore, the interfacial peak shear strength demonstrates a heightened sensitivity to temperature fluctuations within the 20 °C to 40 °C temperature range compared to the other temperature ranges. Furthermore, the interfacial peak shear stress demonstrates a heightened sensitivity to temperature fluctuations at elevated positive stress levels compared to at lower positive stress levels. The friction angle of the marine sand–polymer layer exhibits a discernible temperature-dependent response, with a notable decrease observed as the temperature increases from 5 °C to 40 °C. This results in a reduction in the friction angle, which decreases from 33.3° to 19.8°. As the temperature increases from 40 °C to 80 °C, the friction angle exhibits an increase, reaching 31.7° from its initial value of 19.8°.

The shear dilation angle of the marine sand–geomembrane interface displays a discernible pattern in response to changes in temperature. As the temperature increases from 5 °C to 40 °C, the maximum shear dilation angle of the interface demonstrates a corresponding increase in accordance with the elevated temperature. As the temperature rises from 40 °C to 80 °C, the maximum interfacial shear dilation angle shows a decline in magnitude. The maximum interfacial shear dilatation angle is observed to peak at 40 °C under three distinct normal pressure levels. There is a notable coupling effect between the peak friction angle and the maximum interfacial shear dilatation angle, with the peak shear dilatation angle and the peak friction angle of the marine sand–polymer layer interfaces displaying inverse change relationships under varying experimental conditions.

Author Contributions: Conceptualization, Z.C. and H.Z.; Investigation, Z.C. and H.Z.; Resources, Z.C.; Data curation, Z.C. and P.C.; Writing—review and editing, Z.C., H.L. (Hui Liu), P.C., Y.L.(Yang Lu), D.S., H.L. (Hai Lin), B.H., and S.C.; Supervision, H.Z. and D.S.; Software, H.Z., Y.L., H.L. (Hui Liu), and B.H.; Funding acquisition, S.C. All authors have read and agreed to the published version of the manuscript.

Funding: The authors would like to acknowledge the consistent support of National Natural Science Foundation of China—No 52471290 and No 52301327. This work was funded by National Engineering ResearchCenter of Ship & Shipping Control System and this work was also funded by China Postdoctoral Science Foundation—No 2024T170217 and No 2023M730929; by Failure Mechanics and Engineering Disaster Prevention, Key Lab of Sichuan Province—No FMEDP202209; by Shanghai Sailing Program—No 22YF1415800 and No 23YF1416100; by Shanghai Natural Science Foundation—No 23ZR1426200 and No 24ZR1427900; by The Shanghai Soft Science Key Project—No 23692119700; by Key Laboratory of Ministry of Education for Coastal Disaster and Protection, Hohai University—No 202302; and by Key Laboratory of Estuarine and Coastal Engineering, Ministry of Transport, No KLECE202302.

Institutional Review Board Statement: Not applicable.

Informed Consent Statement: Not applicable.

Data Availability Statement: Data are contained within the article.

Conflicts of Interest: Author Bing Han was employed by the company Shanghai Ship and Shipping Research Institute Co., Ltd. Author Shuang Chen was employed by the company Jiangsu Water Conservancy Engineering Technology Consulting Co., Ltd. The remaining authors declare that the research was conducted in the absence of any commercial or financial relationships that could be construed as a potential conflict of interest.

References

1. Wu, Q.; Liu, Q.; Zhuang, H.; Xu, C.; Chen, G. Experimental investigation of dynamic shear modulus of saturated marine coral sand. *Ocean Eng.* **2022**, *264*, 112412.
2. Peng, Y.; Ding, X.; Yin, Z.-Y.; Wang, P. Micromechanical analysis of the particle corner breakage effect on pile penetration resistance and formation of breakage zones in coral sand. *Ocean Eng.* **2022**, *259*, 111859.
3. Shao, W.; Qin, F.; Shi, D.; Soomro, M.A. Horizontal bearing characteristic and seismic fragility analysis of CFRP composite pipe piles subject to chloride corrosion. *Comput. Geotech.* **2024**, *166*, 105977.
4. Dong, Y.; Wang, D.; Randolph, M.F.J.O.E. Investigation of impact forces on pipeline by submarine landslide using material point method. **2017**, *146*, 21–28.
5. Wu, Q.; Ding, X.; Zhang, Y.; Chen, Z.; Zhang, Y. Numerical simulations on seismic response of soil-pile-superstructure in coral sand. *Ocean Eng.* **2021**, *239*, 109808.
6. Wang, P.; Yin, Z.Y.; Hicher, P.Y.; Cui, Y.J. Micro-mechanical analysis of one-dimensional compression of clay with DEM. *Int. J. Numer. Anal. Methods Geomech.* **2023**, *47*, 2706–2724.
7. Rowe, R.K.; Fan, J. A general solution for leakage through geomembrane defects overlain by saturated tailings and underlain by highly permeable subgrade. *Geotext. Geomembr.* **2022**, *50*, 694–707.
8. Rowe, R.K.; Fan, J. Effect of geomembrane hole geometry on leakage overlain by saturated tailings. *Geotext. Geomembr.* **2021**, *49*, 1506–1518.
9. Zhou, B.; Ku, Q.; Li, C.; Wang, H.; Dong, Y.; Cheng, Z. Single-particle crushing behaviour of carbonate sands studied by X-ray microtomography and a combined finite–discrete element method. *Acta Geotech.* **2022**, *17*, 3195–3209.
10. Zhang, Y.; Zang, W.; Zheng, J.; Cappietti, L.; Zhang, J.; Zheng, Y.; Fernandez-Rodriguez, E. The influence of waves propagating with the current on the wake of a tidal stream turbine. *Appl. Energy* **2021**, *290*, 116729.
11. Zhang, Y.; Zhang, Z.; Zheng, J.; Zheng, Y.; Zhang, J.; Liu, Z.; Fernandez-Rodriguez, E. Research of the array spacing effect on wake interaction of tidal stream turbines. *Ocean Eng.* **2023**, *276*, 114227.
12. Zhao, G.; Wu, T.; Ren, G.; Zhu, Z.; Gao, Y.; Shi, M.; Ding, S.; Fan, H. Reusing waste coal gangue to improve the dispersivity and mechanical properties of dispersive soil. *J. Clean. Prod.* **2023**, *404*, 136993.
13. Zhao, G.; Zhu, Z.; Ren, G.; Wu, T.; Ju, P.; Ding, S.; Shi, M.; Fan, H. Utilization of recycled concrete powder in modification of the dispersive soil: A potential way to improve the engineering properties. *Constr. Build. Mater.* **2023**, *389*, 131626.
14. Zheng, Z.; Xu, H.; Zhang, K.; Feng, G.; Zhang, Q.; Zhao, Y. Intermittent disturbance mechanical behavior and fractional deterioration mechanical model of rock under complex true triaxial stress paths. *Int. J. Min. Sci. Technol.* **2024**, *34*, 117–136.
15. Zheng, Z.; Deng, B.; Li, S.; Zheng, H. Disturbance mechanical behaviors and anisotropic fracturing mechanisms of rock under novel three-stage true triaxial static-dynamic coupling loading. *Rock Mech. Rock Eng.* **2024**, *57*, 2445–2468.
16. Zhao, S.; Zhang, J.; Feng, S.-J. The era of low-permeability sites remediation and corresponding technologies: A review. *Chemosphere* **2023**, *313*, 137264.

17. Chao, Z.; Shi, D.; Zheng, J. Experimental research on temperature–Dependent dynamic interface interaction between marine coral sand and polymer layer. *Ocean Eng.* **2024**, *297*, 117100.
18. Zhang, W.; Li, H.; Shi, D.; Shen, Z.; Zhao, S.; Guo, C. Determination of Safety Monitoring Indices for Roller-Compacted Concrete Dams Considering Seepage–Stress Coupling Effects. *Mathematics* **2023**, *11*, 3224.
19. Chen, W.-B.; Xu, T.; Zhou, W.-H. Microanalysis of smooth Geomembrane–Sand interface using FDM–DEM coupling simulation. *Geotext. Geomembr.* **2021**, *49*, 276–288.
20. Ari, A.; Akbulut, S. Evaluation of sand-geomembrane interface behavior using discrete element method. *Granul. Matter* **2022**, *24*, 1–21.
21. Anjana, R.; Keerthana, S.; Arnepalli, D.N. Coupled effect of UV ageing and temperature on the diffusive transport of aqueous, vapour and gaseous phase organic contaminants through HDPE geomembrane. *Geotext. Geomembr.* **2023**, *51*, 316–329.
22. Francey, W.; Rowe, R.K. Importance of thickness reduction and squeeze-out Std-OIT loss for HDPE geomembrane fusion seams. *Geotext. Geomembr.* **2023**, *51*, 30–42.
23. Bilgin, Ö.; Stewart, H.E.; O'rourke, T.D. Thermal and mechanical properties of polyethylene pipes. *J. Mater. Civ. Eng.* **2007**, *19*, 1043–1052.
24. Chao, Z.; Wang, H.; Hu, S.; Wang, M.; Xu, S.; Zhang, W. Permeability and porosity of light-weight concrete with plastic waste aggregate: Experimental study and machine learning modelling. *Constr. Build. Mater.* **2024**, *411*, 134465.
25. Ren, P.; Chen, Z.-L.; Li, L.; Gong, W.; Li, J. Dynamic shakedown behaviors of flexible pavement overlying saturated ground under moving traffic load considering effect of pavement roughness. *Comput. Geotech.* **2024**, *168*, 106134.
26. Zheng, H.; Zhang, H.; Liang, F.; Li, L. Numerical investigation on lateral monotonic and cyclic responses of scoured rigid monopile based on an integrated bounding surface model. *Comput. Geotech.* **2024**, *166*, 105997.
27. Wang, F.; Zhang, D.; Huang, H.; Huang, Q. A phase-field-based multi-physics coupling numerical method and its application in soil–water inrush accident of shield tunnel. *Tunn. Undergr. Space Technol.* **2023**, *140*, 105233.
28. Wang, F.; Zhou, M.; Shen, W.; Huang, H.; He, J. Fluid-solid-phase multi-field coupling modeling method for hydraulic fracture of saturated brittle porous materials. *Eng. Fract. Mech.* **2023**, *286*, 109231.
29. Xu, J.; Gong, J.; Li, Y.; Fu, Z.; Wang, L. Surf-riding and broaching prediction of ship sailing in regular waves by LSTM based on the data of ship motion and encounter wave. *Ocean Eng.* **2024**, *297*, 117010.
30. Lin, H.; Gong, X.; Zeng, Y.; Zhou, C. Experimental study on the effect of temperature on HDPE geomembrane/geotextile interface shear characteristics. *Geotext. Geomembr.* **2024**, *52*, 396–407.
31. Samea, A.; Abdelaal, F. Effect of elevated temperatures on the degradation behaviour of elastomeric bituminous geomembranes. *Geotext. Geomembr.* **2023**, *51*, 219–232.
32. Xiao, Y.; Wang, Y.; Wang, S.; Evans, T.M.; Stuedlein, A.W.; Chu, J.; Zhao, C.; Wu, H.; Liu, H. Homogeneity and mechanical behaviors of sands improved by a temperature-controlled one-phase MICP method. *Acta Geotech.* **2021**, *16*, 1417–1427.
33. Cui, J.; Jin, Y.; Jing, Y.; Lu, Y. Elastoplastic Solution of Cylindrical Cavity Expansion in Unsaturated Offshore Island Soil Considering Anisotropy. *J. Mar. Sci. Eng.* **2024**, *12*, 308.
34. Zhang, X.; Zhai, E.; Wu, Y.; Sun, D.a.; Lu, Y. Theoretical and numerical analyses on hydro–thermal–salt–mechanical interaction of unsaturated salinized soil subjected to typical unidirectional freezing process. *Int. J. Geomech.* **2021**, *21*, 04021104.
35. He, S.-H.; Shan, H.-F.; Xia, T.-D.; Liu, Z.-J.; Ding, Z.; Xia, F. The effect of temperature on the drained shear behavior of calcareous sand. *Acta Geotech.* **2021**, *16*, 613–633.
36. Shu, Z.; You, R.; Xie, Y. Viscoelastic Dampers for Vibration Control of Building Structures: A State-of-Art Review. *J. Earthq. Eng.* **2024**, *28*, 3558–3585. https://doi.org/10.1080/13632469.2024.2345180.
37. Li, T.; Zhu, Z.; Wu, T.; Ren, G.; Zhao, G. A potential way for improving the dispersivity and mechanical properties of dispersive soil using calcined coal gangue. *J. Mater. Res. Technol.* **2024**, *29*, 3049–3062.
38. Rotta Loria, A.; Coulibaly, J. Thermally induced deformation of soils: A critical overview of phenomena, challenges and opportunities. *Geomech. Energy Environ.* **2020**, *25*, 100193.
39. Bilgin, Ö.; Shah, B. Temperature influence on high-density polyethylene geomembrane and soil interface shear strength. *Int. J. Geosynth. Ground Eng.* **2021**, *7*, 1–10.
40. Dong, Y.; Liao, Z.; Wang, J.; Liu, Q.; Cui, L. Potential failure patterns of a large landslide complex in the Three Gorges Reservoir area. *Bull. Eng. Geol. Environ.* **2023**, *82*, 41.
41. Ma, W.; Liu, Z.; Zhu, T.; Wang, L.; Du, J.; Wang, K.; Xu, C. Fabric-Enhanced Vascular Graft with Hierarchical Structure for Promoting the Regeneration of Vascular Tissue. *Adv. Healthc. Mater.* **2024**, *13*, 2302676.
42. Xiao, G.; Xu, L. Challenges and Opportunities of Maritime Transport in the Post-Epidemic Era. *J. Mar. Sci. Eng.* **2024**, *12*, 1685.
43. Cheng, Z.; Wang, J.; Xiong, W. A machine learning-based strategy for experimentally estimating force chains of granular materials using X-ray micro-tomography. *Géotechnique* **2024**, *74*, 1291–1303. https://doi.org/10.1680/jgeot.21.00281.
44. Chao, Z.; Dang, Y.; Pan, Y.; Wang, F.; Wang, M.; Zhang, J.; Yang, C. Prediction of the shale gas permeability: A data mining approach. *Geomech. Energy Environ.* **2023**, *33*, 100435.
45. Karademir, T.; Frost, J.D. Micro-scale tensile properties of single geotextile polypropylene filaments at elevated temperatures. *Geotext. Geomembr.* **2014**, *42*, 201–213.
46. Karademir, T.; Frost, J.D. Elevated temperature effects on geotextile–geomembrane interface shear behavior. *J. Geotech. Geoenviron. Eng.* **2021**, *147*, 04021148.

47. Zhang, X.; Zhang, L.; Wu, J.; Fu, H.; Dian, L. Tunnel stability analysis of coral reef limestone stratum in ocean engineering. *Ocean Eng.* **2022**, *265*, 112636.
48. Wang, P.; Xu, C.; Yin, Z.-Y.; Song, S.-x.; Xu, C.; Dai, S. A DEM-based Generic Modeling Framework for Hydrate-Bearing Sediments. *Comput. Geotech.* **2024**, *171*, 106287.
49. Liu, Y.; Wang, L.; Liu, Z.; Kang, Y.; Chen, T.; Xu, C.; Zhu, T. Durable Immunomodulatory Nanofiber Niche for the Functional Remodeling of Cardiovascular Tissue. *ACS Nano* **2024**, *18*, 951–971. https://doi.org/10.1021/acsnano.3c09692.
50. Ceccato, F.; Yerro, A.; Girardi, V.; Simonini, P. Two-phase dynamic MPM formulation for unsaturated soil. *Comput. Geotech.* **2021**, *129*, 103876.
51. Zhao, Y.; Yang, Y.; Ling, X.; Gong, W.; Li, G.; Su, L. Dynamic behavior of natural sand soils and fiber reinforced soils in heavy-haul railway embankment under multistage cyclic loading. *Transp. Geotech.* **2021**, *28*, 100507.
52. Mahigir, A.; Ardakani, A.; Hassanlourad, M. Comparison between monotonic, cyclic and post-cyclic pullout behavior of a PET geogrid embedded in clean sand and clayey sand. *Int. J. Geosynth. Ground Eng.* **2021**, *7*, 1–15.
53. Cardile, G.; Pisano, M.; Moraci, N. The influence of a cyclic loading history on soil-geogrid interaction under pullout condition. *Geotext. Geomembr.* **2019**, *47*, 552–565.
54. Samanta, M.; Bhowmik, R.; Khanderi, H. Laboratory evaluation of dynamic shear response of sand–geomembrane interface. *Geosynth. Int.* **2022**, *29*, 99–112.
55. Zeng, W.-x.; Ying, M.-j.; Liu, F.-y. Investigation on the cyclic shear response of stereoscopic geogrid-reinforced coarse-grained soil interface. *Transp. Geotech.* **2023**, *38*, 100905.
56. Chao, Z.; Wang, H.; Zheng, J.; Shi, D.; Li, C.; Ding, G.; Feng, X. Temperature-Dependent Post-Cyclic Mechanical Characteristics of Interfaces between Geogrid and Marine Reef Sand: Experimental Research and Machine Learning Modeling. *J. Mar. Sci. Eng.* **2024**, *12*, 1262.
57. Wang, J.; Liu, F.; Wang, P.; Cai, Y. Particle size effects on coarse soil-geogrid interface response in cyclic and post-cyclic direct shear tests. *Geotext. Geomembr.* **2016**, *44*, 854–861.
58. Ying, M.; Liu, F.; Wang, J.; Wang, C.; Li, M. Coupling effects of particle shape and cyclic shear history on shear properties of coarse-grained soil–geogrid interface. *Transp. Geotech.* **2021**, *27*, 100504.
59. Chao, Z.; Wang, H.; Hu, H.; Ding, T.; Zhang, Y. Predicting the temperature-dependent long-term creep mechanical response of silica sand-textured geomembrane interfaces based on physical tests and machine learning techniques. *Materials* **2023**, *16*, 6144.
60. Chao, Z.; Yang, C.; Zhang, W.; Zhang, Y.; Zhou, J. Predicting the Gas Permeability of Sustainable Cement Mortar Containing Internal Cracks by Combining Physical Experiments and Hybrid Ensemble Artificial Intelligence Algorithms. *Materials* **2023**, *16*, 5330.
61. Chao, Z.; Fowmes, G.; Mousa, A.; Zhou, J.; Zhao, Z.; Zheng, J.; Shi, D. A new large-scale shear apparatus for testing geosynthetics-soil interfaces incorporating thermal condition. *Geotext. Geomembr.* **2024**, *52*, 999–1010.
62. El Naggar, H.; Zahran, K.; Moussa, A. Effect of the particle size on the TDA shear strength and stiffness parameters in large-scale direct shear tests. *Geotechnics* **2021**, *1*, 1–17.
63. Howard, A.K. The revised ASTM standard on the unified classification system. *Geotech. Test. J.* **1984**, *7*, 216-222.
64. Kalasin, T.; Khamchan, C.; Aoddej, A. Effects of particle size and soil bed on the shear strength of materials in the direct shear test. *Period. Polytech. Civ. Eng.* **2023**, *67*, 166–176.
65. Altun, S.; Göktepe, B.; Sezer, A. Relationships between shape characteristics and shear strength of sands. *Soils Found.* **2011**, *51*, 857–871.
66. Daghistani, F.; Abuel-Naga, H. Evaluating the influence of sand particle morphology on shear strength: A comparison of experimental and machine learning approaches. *Appl. Sci.* **2023**, *13*, 8160.
67. Viggiani, G.; Küntz, M.; Desrues, J. An experimental investigation of the relationships between grain size distribution and shear banding in sand. *Contin. Discontinuous Model. Cohesive-Fract. Mater.* **2001**, *568*, 111–127.
68. Chao, Z.; Liu, H.; Wang, H.; Dong, Y.; Shi, D.; Zheng, J. The interface mechanical properties between polymer layer and marine sand with different particle sizes under the effect of temperature: Laboratory tests and artificial intelligence modelling. *Ocean Eng.* **2024**, *312*, 119255.
69. Kuang, D.; Long, Z.; Guo, R.; Yu, P. Experimental and numerical investigation on size effect on crushing behaviors of single calcareous sand particles. *Mar. Georesour. Geotechnol.* **2021**, *39*, 543–553.
70. Wang, X.; Wu, Y.; Cui, J.; Zhu, C.-Q.; Wang, X.-Z. Shape characteristics of coral sand from the South China Sea. *J. Mar. Sci. Eng.* **2020**, *8*, 803.
71. Chao, Z.; Li, Z.; Dong, Y.; Shi, D.; Zheng, J. Estimating compressive strength of coral sand aggregate concrete in marine environment by combining physical experiments and machine learning-based techniques. *Ocean Eng.* **2024**, *308*, 118320.
72. Abdelaal, F.; Rowe, R.K.; Morsy, M.; e Silva, R.J.G.; Geomembranes. Degradation of HDPE, LLDPE, and blended polyethylene geomembranes in extremely low and high pH mining solutions at 85 °C. *Geotext. Geomembr.* **2023**, *51*, 27–38.
73. Rowe, R.K.; Sangam, H.P.J.G.; Geomembranes. *Durab. HDPE Geomembr.* **2002**, *20*, 77–95.
74. Lavoie, F.L.; Kobelnik, M.; Valentin, C.A.; Silva, J.L.d.J.Q.N. Durability of HDPE geomembranes: An overview. *Quim. Nova* **2020**, *43*, 656–667.
75. Ghazizadeh, S.; Bareither, C.A. Effect of temperature on critical strength of geosynthetic clay liner/textured geomembrane composite systems. *Geotext. Geomembr.* **2024**, *52*, 12–26.

76. SoilGeosynthetic, D.D.S.T.M.f.D.t.S.S.o.; D/DM, G.I.b.D.S.h.b.r.t. D5321 Standard Test Method for Determining the Shear Strength of Soil-Geosynthetic and Geosynthetic-Geosynthetic Interfaces by Direct Shear has been revised (with title change) to D5321-12. Astm.
77. Fleming, I.; Sharma, J.; Jogi, M. Shear strength of geomembrane–soil interface under unsaturated conditions. *Geotext. Geomembr.* **2006**, *24*, 274–284.
78. Zhao, H.; Tian, K. Shear strength of HDPE smooth geomembrane/bentonite-polymer geosynthetic clay liner interface. *Geotext. Geomembr.* **2023**, *51*, 73–86.
79. Araújo, G.L.S.; Sánchez, N.P.; Palmeira, E.M.; de Almeida, M.d.G.G. Influence of micro and macroroughness of geomembrane surfaces on soil-geomembrane and geotextile-geomembrane interface strength. *Geotext. Geomembr.* **2022**, *50*, 751–763.
80. Cen, W.; Bauer, E.; Wen, L.; Wang, H.; Sun, Y. Experimental investigations and constitutive modeling of cyclic interface shearing between HDPE geomembrane and sandy gravel. *Geotext. Geomembr.* **2019**, *47*, 269–279.
81. Shoushtari, M.; Lashkari, A.; Martinez, A. Effect of gas-oil contamination on the mechanical behavior of sand-woven geotextile interface: Experimental investigation and constitutive modeling. *Geotext. Geomembr.* **2023**, *51*, 56–71.
82. Standard Practice for Obtaining Samples of Geosynthetic Clay Liners. 2019, ASTM D6072/D6072M-19e1.
83. Chao, Z.; Fowmes, G.; Dassanayake, S. Comparative study of hybrid artificial intelligence approaches for predicting peak shear strength along soil-geocomposite drainage layer interfaces. *Int. J. Geosynth. Ground Eng.* **2021**, *7*, 60.
84. Chao, Z.; Shi, D.; Fowmes, G.; Xu, X.; Yue, W.; Cui, P.; Hu, T.; Yang, C. Artificial intelligence algorithms for predicting peak shear strength of clayey soil-geomembrane interfaces and experimental validation. *Geotext. Geomembr.* **2023**, *51*, 179–198.
85. Chao, Z.; Shi, D.; Fowmes, G.J.E.G. Mechanical behaviour of soil under drying–wetting cycles and vertical confining pressures. *Environ. Geotech.* **2023**, *40*, 1–11.
86. Shi, D.; Niu, J.; Zhang, J.; Chao, Z.; Fowmes, G. Effects of particle breakage on the mechanical characteristics of geogrid-reinforced granular soils under triaxial shear: A DEM investigation. *Geomech. Energy Environ.* **2023**, *34*, 100446.
87. Dassanayake, S.; Mousa, A.; Fowmes, G.J.; Susilawati, S.; Zamara, K. Forecasting the moisture dynamics of a landfill capping system comprising different geosynthetics: A NARX neural network approach. *Geotext. Geomembr.* **2023**, *51*, 282–292.